J Mol Model (2012) 18:4381–4387
DOI 10.1007/s00894-012-1444-x

ORIGINAL PAPER

Induced chirality in fisetin upon binding to serum albumin: experimental circular dichroism and TDDFT calculations

Iulia Matei · Sorana Ionescu · Mihaela Hillebrand

Received: 23 January 2012 / Accepted: 19 April 2012 / Published online: 15 May 2012

Abstract Theoretical absorption and electronic circular dichroism (ECD) spectra predicted via time-dependent density functional theory (TDDFT) calculations on the neutral and four anionic species of fisetin, an achiral flavonoid, were used to rationalize the experimental absorption and induced circular dichroism (ICD) spectra of the ligand upon binding to human serum albumin (HSA). On this basis, the mechanism responsible for the appearance of the ICD signal was ascribed to a distortion of the conformation of bound fisetin. Furthermore, comparison of the simulated and experimental spectra revealed that two fisetin species bind to HSA, namely, the neutral molecule and the anion deprotonated at the hydroxyl group in position 7, in a 1:1 ratio. The coupling of the theoretical results with the experimental absorption and ICD data allows identification of the flavonoid species that bind to the protein and evaluation of their conformation in the binding site.

Keywords Flavonoid · Human serum albumin · Induced circular dichroism · Time-dependent density functional calculations · Fisetin anionic species

Introduction

Quantum chemistry methods are used successfully to determine molecular structure as an auxiliary tool to experimental spectroscopic determinations. Some of their main purposes are to ascribe vibrational modes in the IR or Raman spectrum [1], to determine the absolute configuration of chiral compounds [2, 3] and to identify the molecular structure of reactants and reaction intermediates [4, 5]. A more recent application was to determine the geometry and species of binding ligand in the pocket of a protein by simulating the induced circular dichroism spectrum of the ligand observed upon interaction [6].

Circular dichroism [7], both electronic (ECD) and vibrational, has been used widely as a spectroscopic tool in determining absolute configurations of organic compounds [8, 9], secondary structure of (bio)polymers [10, 11] and ligand binding parameters [12]. An interesting effect arises when an achiral chromophore interacts with a chiral compound. The chromophore becomes optically active, a phenomenon referred to as induced circular dichroism (ICD) [13]. ICD has proven to be a powerful technique for studies of interactions of achiral organic molecules with the surrounding media, from chiral solvents [14, 15] to large systems such as (bio)polymers [16–19], cyclodextrins [20–22] and supramolecular structures like micelles [23]. The ICD effect occurs in the light-absorbing region of the ligand and has more features than the absorption spectrum. It is characterized not only by the position and intensity of the bands but also by a positive or negative sign [7]. These make the ICD signal very sensitive to conformational changes of the ligand in the restricted environment of the binding site of a protein, and thus an appropriate technique to obtain structural information. The problem becomes more complex in the case of easily ionizable compounds undergoing multiple acid–base equilibria in the buffer media used for studying ligand–protein interactions. One of the issues that must be overcome is to determine which of the species present in the system are effectively included in the binding pocket of the

Electronic supplementary material The online version of this article (doi:10.1007/s00894-012-1444-x) contains supplementary material, which is available to authorized users.

I. Matei · S. Ionescu (✉) · M. Hillebrand
Department of Physical Chemistry, University of Bucharest,
Bd. Regina Elisabeta 4-12,
030018 Bucharest, Romania
e-mail: sorana@gw-chimie.math.unibuc.ro

protein. Quantum chemistry methods can play a decisive role in ascribing the experimental ICD spectrum of the bound ligand to the respective species and conformation by simulating the ECD spectrum of all the possible species adopting several relevant conformations and choosing the one(s) matching the experiment.

The present paper continues our earlier work on characterizing the flavonoid–human serum albumin (HSA) interaction [24, 25]. The flavonoid chosen in this study is fisetin, belonging to the flavonol class (Fig. 1). We have previously characterized its interaction with HSA in terms of determining the stoichiometry (1:1), localizing the binding site (Sudlow I), determining the binding constant (1×10^{-5} M^{-1}), energy transfer efficiency and loss in α-helix content of HSA upon binding. The methods employed were steady-state and time-resolved fluorescence and circular dichroism on the intrinsic band of HSA [25].

In the present paper, we aimed to use theoretical density functional theory (DFT) methods in order to rationalize the experimental features of the absorption and ICD spectra of fisetin and, on this basis, to determine the species that binds to HSA and its conformation in the binding pocket. The calculations were performed on neutral fisetin as well as on all the possible anionic species considering several conformations that can be adopted in the protein binding pocket.

The procedure consists of three steps. Firstly, a high level theoretical characterisation of all species presumed to exist in the system. This includes determination of the minimum point energy, Boltzmann population, main points on the potential energy curve (built along the internal coordinate that determines the conformational change upon binding) and, for the significant geometries of each species, calculation of the UV and ECD spectra. Secondly, the deconvolution of the UV and ECD experimental spectra in the absence and presence of the protein, in order to obtain the positions of the maxima and the relative intensities of all components; the comparison of these data with the theoretically estimated Boltzmann populations and the TDDFT calculated spectra for all the presumed species allows for identification of the binding species. In the third step, a convolution of the overall spectrum is undertaken, considering different proportions for the binding species. The comparison of this simulated spectrum with the experimental one gives the ratio of the species involved in the binding process. The results obtained can be used as a more reliable starting point in the further modeling of the entire ligand–protein system.

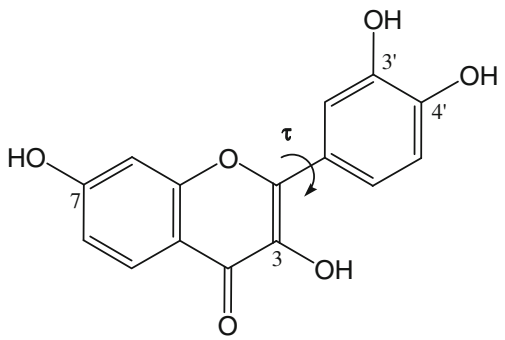

Fig. 1 Molecular structure of fisetin and numbering of ring positions

Material and methods

Absorption and circular dichroism measurements

A solution of 3.5×10^{-5} M fisetin in ethanol:phosphate buffer of pH 7.4 1:9 v:v was prepared for absorption measurements. Several fisetin–HSA solutions were obtained in the range of drug to protein (d/p) molar ratio 0–1, such as to ensure a constant 7.5×10^{-5} M HSA concentration. We checked that no changes in the HSA absorption and CD spectra occur in presence of up to 20 % ethanol. CD and absorption spectra were recorded on a Jasco J-815 CD spectropolarimeter at 25 °C in the wavelength range 250–500 nm. The ICD signal of complexed fisetin, $\Delta\theta$, expressed as ellipticity in millidegrees (mdeg), was corrected by subtracting at each wavelength the CD of HSA and fisetin alone from the spectrum of the complex.

Theoretical calculations

The geometry optimization of fisetin was carried out by density functional theory (DFT) calculations using the B3LYP functional [26–28] and the 6-31++G(d,p) basis set in the frame of the Gaussian03 package [29]. The solvent (water) effect was introduced by the Polarizable Continuum Model [30]. Calculations were performed on the neutral (N) and four anionic species of fisetin (anions deprotonated at the hydroxyls in positions 3, 7, 3′ and 4′, hereinafter named A3, A7, A3′ and A4′, respectively) for which several conformations were obtained by modifying the torsion angle τ (Fig. 1) in the range 0–90 °. The Gibbs free energy as given by Gaussian03 subsequent to a vibrational analysis at the same level of theory is used. It includes the zero-point correction and the thermal correction for the Gibbs free energy at 298.15 K and was used to calculate the relative Bolzmann population of the anions.

The simulated absorption and CD spectra of the aforementioned conformers were computed by time-dependent DFT (TDDFT), B3LYP/6-31++G(d,p), and plotted employing Gabedit 2.3.5 [31], with a full width at half maximum of 15 nm. The simulated absorption spectrum of free fisetin in solution was obtained by reconvolution of the theoretical spectra of different conformations (with a step of 20 ° for the

dihedral τ), weighted by the respective Boltzmann population. We checked that the CD spectrum for a negative τ value is the mirror-image of that for a positive value.

Results and discussion

Experimental absorption and induced CD spectra of fisetin upon binding to HSA

The experimental data needed in order to determine the changes induced by binding are both the ICD and absorption spectra. As fisetin is achiral and has an ICD signal only in the presence of HSA, the absorption spectrum of fisetin allows one to estimate the wavelength corresponding to the electronic transitions of free fisetin and to compare it to those of the fisetin–HSA complex. On the other hand, the ICD spectrum, having positive and negative bands, is more sensitive to conformational changes of the ligand in the binding pocket so it is more appropriate to estimate the conformation of the bound ligand.

Fisetin has four hydroxyl groups that can each be subject to an acido–basic equilibrium yielding an anion. The first pKa value of fisetin is $pKa_1=7.4$ [32], which is considered to correspond to the deprotonation of the hydroxyl group in position 7. In phosphate buffer at pH 7.4 fisetin exists both as N and A7 forms, but the equilibrium of species can be more complex at basic pH values ($pKa_2=9.4$; the rest are difficult to determine [32]). For neutral fisetin, the absorption band located at 375 nm is ascribed in the literature to the electronic transitions involving the cinnamoyl molecular fragment [12, 33]. The deconvolution of the absorption spectrum at pH 7.4 is presented in Fig. 2a and reveals the presence of five bands, with maxima at 263, 314, 377, 422, 469 nm corresponding to different species, neutral and anionic, present in solution, that will be ascribed on grounds of the simulated spectra.

Figure 2b presents the deconvolution of the absorption spectrum of the 1:1 fisetin:HSA mixture. The band at 283 nm corresponds to the protein—more precisely to the tryptophan and tyrosine residues. One can see that, upon binding to HSA, the band at 469 nm disappears. A new band appears at 331 nm. The other bands are shifted slightly compared to unbound fisetin, the maxima being at 268, 307, 378 and 417 nm. Moreover, the intensity ratio of the bands at 422 (shifted to 417) nm and 377 (378) nm increases, while the band at 469 nm does not appear at all. One can conclude from these features that the deprotonation equilibrium is perturbed by the binding process and that the neutral:anions ratio changes.

Regarding the CD spectrum, planar fisetin is optically inactive and, due to the unhindered rotation of the chromone and phenyl fragments about the single bond, no CD band is observed when free in solution. However, important changes in the CD spectrum were observed upon binding to chiral HSA, which provides a rigid environment for the ligand (Fig. 3a). When the d/p ratio increases from 0 to 1, an ICD signal appears that can be explained by the following mechanism. As fisetin is included in the binding pocket of HSA, due to the limited space within it, rotation between the molecular fragments is hindered and the ligand adopts a distorted conformation. This gives rise to an asymmetry and thus to the appearance of ICD bands. Their sign and position are very sensitive to the molecular structure of the bound ligand [6, 34].

We focused our attention on the ICD bands located at wavelengths above 300 nm, as below this spectral range uncertainties arise due to the superposition of the intrinsic dichroic bands corresponding to the n–π* and π–π* transitions of the amide groups and aromatic residues of HSA [35]. The ICD spectrum of the fisetin:HSA system exhibits four bands in the absorption region of fisetin, all of which are negative. Their maxima are at 322, 335, 378 and 411 nm, as revealed from the deconvolution in Fig. 3b, and differ slightly from the absorption maxima of the fisetin:HSA mixture obtained by deconvolution (vide supra). The differences may originate in the fact that the absorption spectrum corresponds to both free and bound fisetin species,

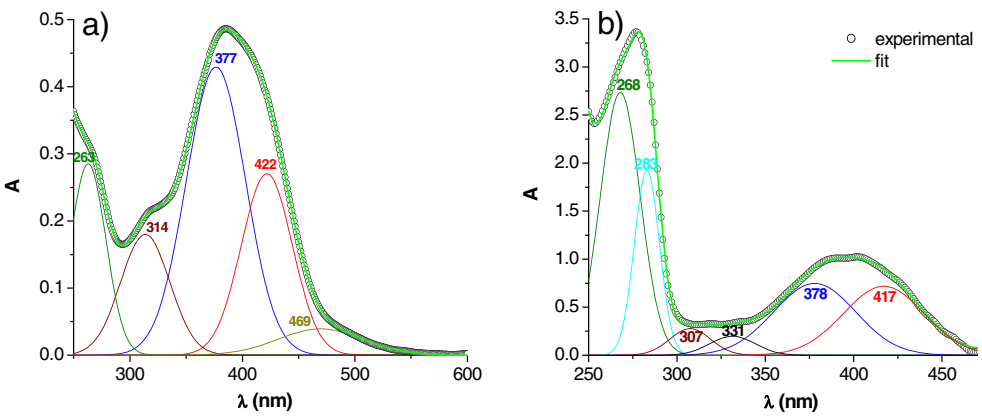

Fig. 2 The deconvoluted absorption spectra of **a** 3.5×10^{-5} M fisetin in ethanol: phosphate buffer of pH 7.4 1:9 v:v, and **b** a 1:1 fisetin:human serum albumin (HSA) mixture

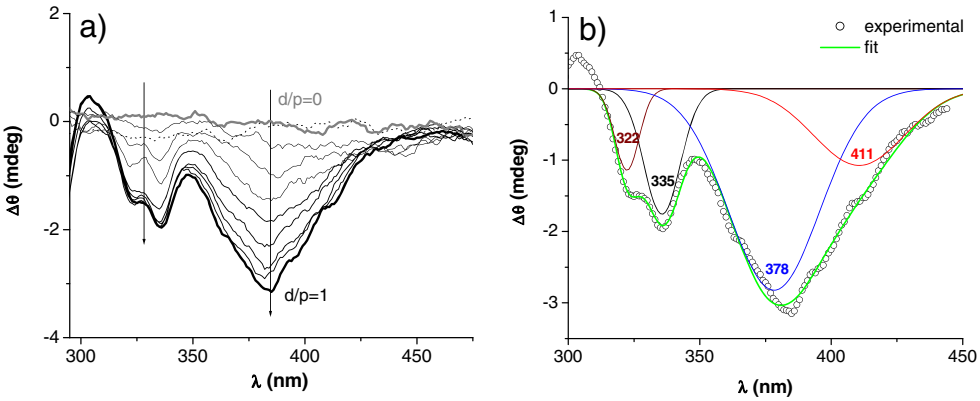

Fig. 3 **a** Induced circular dichroism (ICD) spectra of the fisetin:HSA system at different d/p values in the range 0–1; [HSA]=7.5×10^{-5} M in pH 7.4 buffer; dotted spectrum: [fisetin]=7.5×10^{-5} M in ethanol:phosphate buffer 1:4 v:v. **b** Deconvolution of the spectrum at d/p=1

while only bound species have an ICD signal. The assignment of these bands and evidencing of the binding fisetin species will be made on the basis of theoretical calculations.

Time-dependent density functional theory calculations

The correlation between experimental and simulated spectra of different possible species of fisetin in several conformations allows both the species and conformation of the bound ligand to be identified [6]. All calculations were performed on the isolated ligand molecule situated in a polarizable continuum. Clearly, the ICD signal originates to a variable extent in both the distortion of the geometry of the ligand in the binding site and the interaction between the transition moments of chromophores from the ligand and protein. The present approach considers only the effect of geometry distortion. The literature data on HSA binding of the flavonoid quercetin [36] show that the asymmetry element correlated with the occurrence of ICD bands is the dihedral around the chromone and phenyl molecular fragments (τ in Fig. 1).

The optimized geometry of the neutral molecule has τ=15 °. As previously stated, fisetin exists at pH 7.4 as both neutral and anionic forms in solution and the experimental spectrum reflects this behavior. This prompted us to optimize all possible monoanionic forms and simulate their absorption and electronic CD (ECD) spectra corresponding to different conformations. Table 1 presents the relative Gibbs' free energy of the anions, together with the dihedrals τ for the optimized conformation. The most stable anions correspond to the deprotonation of the hydroxyl in position 4′ or 7, which, from the calculated Boltzmann populations, appear as the only ones present in solution. Nonetheless, anion 4′ exhibits two conformers, the most stable one, 4′a, and another one 13.15 kJ mol^{-1} higher, 4′b, that differ in the orientation of the hydroxylic hydrogen at position 3′. This being free to rotate, it is reasonable to think that the population of this anion is Boltzmann averaged between these two conformers.

Table 1 Relative Gibbs' free energy of the anionic forms of fisetin and the respective relative Boltzmann populations

Species	τ (deg)	G_{rel} (kJ/mol)	Relative populations[a]
A7	15	1.47	0.55
A4′a	9	0.00	1.00
A4'b	9	13.15	0.01
A3	1	20.19	0.00
A3′	20	11.82	0.01

[a] From the calculated Gibbs free energies, relative to the most stable anion, considered 1

The intensity and position of the simulated absorption and ECD bands depend strongly on the magnitude of the torsion τ. Figure 4a shows the simulated absorption spectra of N, A7 and A4′, obtained by the reconvolution of the Boltzmann averaged spectra of different conformers (for their individual spectra see Fig. S2 in the Online Resource). The calculations predict three transitions at 378 nm, 296 and 269 nm for the optimized geometry of the neutral molecule, in good agreement with the deconvolution of the experimental spectrum of fisetin in pH 7.4 buffer regarding both the positions (377, 314, 263 nm) and relative intensities of the absorption bands. They are of π–π* character. The band at 378 nm corresponds mainly to the homo–lumo transition, the orbitals involved being localized mostly on the cinnamoyl fragment (see Fig. S1 in the Online Resource). The band at 296 nm corresponds to a homo-2-lumo transition, located on the benzoyl fragment and the one at 269 nm to homo–lumo+1, delocalized on the entire molecule. The anions that best correlate with the position of the experimental bands found by deconvolution (Fig. 2a) are A7 (410 nm) and A4′ (462 nm), i.e., the most stable ones. The oscillator strengths for these three bands are 0.55, 0.37 and 0.79, respectively. When comparing them to the absorbance in the experimental spectrum at the same wavelength (0.48, 0.44 and 0.10), the molar ratio in solution can be estimated as about N:A7:A4′=0.40:0.55:0.05. Therefore, although the most stable anions are A4′ and then A7, 1.47 kJ mol^{-1} higher, the correlation between the experimental and theoretical spectra reveals that A7 is predominant in solution and A4′ is present in small amounts. This means that the DFT

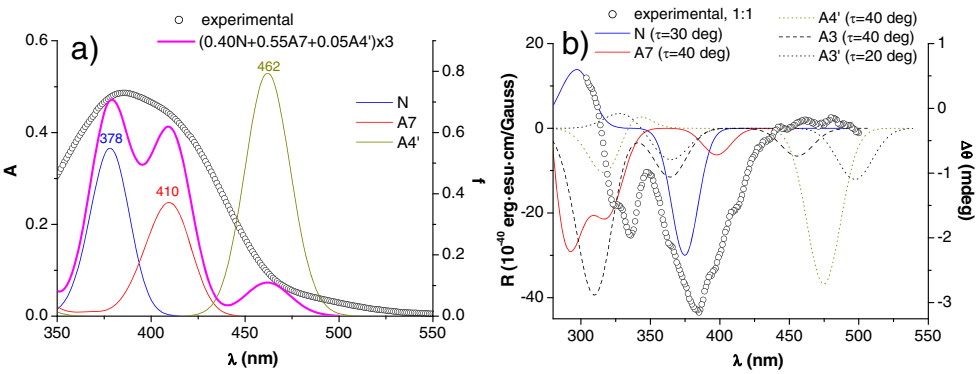

Fig. 4 **a** Simulated absorption spectra of neutral fisetin and its two most stable anions, and their weighted reconvolution that best fits the experimental absorbances. **b** Electronic circular dichroism (ECD) spectra of the neutral and four anionic species of fisetin

calculated populations are only in qualitative agreement with the experimental data, because they predict the species present in solution, but not their real proportion. This most probably originates in the well known errors in the calculated free energy and oscillator strength yielded by DFT methods [37, 38].

The ECD spectra for the neutral and all the anionic species (see Fig. S3 in the Online Resource for several conformations) were calculated as a function of τ. In general, when τ increases the bands shift bathochromically, except for A4′, the intensity increases, reaches a maximum for the most asymmetric conformations (40–60 °) and then decreases, while the sign of the bands is generally not changed. These spectra can be compared to the experimental ICD spectrum in presence of HSA at d/p=1 that was previously deconvoluted in Fig. 3b. Figure 4b presents the spectra of the conformations that best match the wavelength of the experimental bands. Their τ values are 30–40 °, in agreement with literature docking results on the conformation that flavonoids adopt when bound to a protein [12, 39]. One can observe that the species presenting bands only in the range of 300–425 nm are N and A7. The other anions are predicted to have maxima at wavelengths longer than 450 nm, where bound fisetin has no signal. So, most probably, the binding species are N and A7 and we aim to estimate the ratio in which they bind.

Figure 5 shows the shape of the simulated ECD spectrum of previously chosen conformations of N and A7 fisetin at several molar ratios. The position and intensity of the experimental ICD bands for the 1:1 fisetin:HSA mixture, relative to that at 385 nm, are also depicted as vertical lines. The molar ratio that best correlates with the experimental intensities is 0.5:0.5 (blue). Thus, N and A7 bind to the protein in a 1:1 proportion. There is no obvious feature to make one suppose that A4′ binds to HSA as well. It is possible that the hydroxylic proton at position 3′ is involved in a hydrogen bond with an amino acid residue, thus the most stable A4′a reverts to the 13.15 kJ mol^{-1} higher in energy A4′b, which then converts to the more stable A7 or N.

Although the calculations neglect the intermolecular interaction of the flavonoid with HSA, they give a reasonable explanation for the observation of the ICD signal and offer valuable insight on the species and conformation of the flavonoid that binds to the protein, which are not always those in solution. This method that combines experimental ICD data for a drug binding to a protein with theoretical calculations for the isolated molecule can be extended for other protein–ligand systems.

Conclusions

The correlation between the experimental and simulated spectra reveals that fisetin exists as neutral and two anionic species in buffered solution at pH 7.4. The calculated wavelengths for the electronic transitions of the most stable anionic species are close to the experimental values found by deconvolution. In the presence of HSA, the shape of the absorption spectrum changes, but it is difficult to ascertain the bound species. This can be done with the aid of the ICD

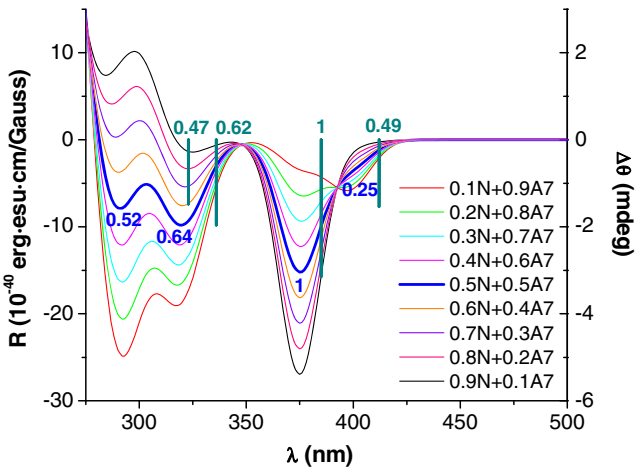

Fig. 5 Reconvolution of the simulated ECD spectra of neutral (τ=30 °) and anion 7 (τ=40 °) fisetin in different molar ratios, together with the position and intensity of the experimental ICD spectrum of the 1:1 fisetin:HSA mixture

spectrum of fisetin, which corresponds to the bound species exclusively. A comparison with the simulated ECD spectrum of mixtures of neutral and anion 7 fisetin in different molar ratios reveals that these most probably bind in a 1:1 proportion. Moreover, their geometry is twisted with a dihedral of 30–40 °. This method can give valuable structural information on the binding of drugs to proteins.

Acknowledgment We gratefully acknowledge the financial support from UEFISCDI grant PN II-ID-1914 no. 494/2009. We would also wish to thank Dr. P. Filip (Institute of Organic Chemistry, Romanian Academy) for kindly making the Gaussian03 calculations possible.

References

1. Scott AP, Radom L (1996) Harmonic vibrational frequencies: an evaluation of Hartree-Fock, Møller-Plesset, quadratic configuration interaction, density functional theory, and semiempirical scale factors. J Phys Chem 100:16502–16513. doi:10.1021/jp960976r
2. Stephens PJ, Devlin FJ, Pan JJ (2008) The determination of the absolute configuration of chiral molecules using vibrational circular dichroism (VCD) spectroscopy. Chirality 20:643–663. doi:10.1002/chir.20477
3. Chmielewski M, Cierpucha M, Kowalska P, Kwit M, Frelek J (2008) Structure-chiroptical properties relationship in clavams: an experimental and theoretical study. Chirality 20:621–627. doi:10.1002/chir.20484
4. Shao L, Zhang L, Chen M, Lu H, Zhou M (2001) Reactions of titanium oxides with water molecules. A matrix isolation FTIR and density functional study. Chem Phys Lett 343:178–184. doi:10.1016/S0009-2614(01)00675-3
5. Yang H, Asplund MC, Kotz KT, Wilkens MJ, Frei H, Harris CB (1998) The reaction mechanism of silicon-hydrogen bond activation studied using femtosecond to nanosecond IR spectroscopy and ab initio methods. J Am Chem Soc 120:10154–10165. doi:10.1021/ja980692f
6. Fitos I, Visy J, Zsila F, Bikadi Z, Mady G, Simonyi M (2004) Specific ligand binding on genetic variants of human a1-acid glycoprotein studied by circular dichroism spectroscopy. Biochem Pharmacol 67:679–688. doi:10.1016/j.bcp.2003.09.039
7. Berova N, Nakanishi K, Woody RW (2000) Circular dichroism: principles and applications. Wiley-VCH, New York
8. Superchi S, Giorgio E, Rosini C (2004) Structural determinations by circular dichroism spectra analysis using coupled oscillator methods: an update of the applications of the DeVoe polarizability model. Chirality 16:422–451. doi:10.1002/chir.20056
9. Allenmark S, Gawronski J (2008) Determination of absolute configuration—an overview related to this special issue. Chirality 20:606–608. doi:10.1002/chir.20524
10. Kelly SM, Jess TJ, Price NC (2005) How to study proteins by circular dichroism. Biochim Biophys Acta 1751:119–139. doi:10.1016/j.bbapap.2005.06.005
11. Tian J, Zhao Y, Liu X, Zhao S (2009) A steady-state and time-resolved fluorescence, circular dichroism study on the binding of myricetin to bovine serum albumin. Luminescence 24:386–393. doi:10.1002/bio.1124
12. Zsila F, Bikadi Z, Simonyi M (2003) Probing the binding of the flavonoid, quercetin to human serum albumin by circular dichroism, electronic absorption spectroscopy and molecular modelling methods. Biochem Pharmacol 65:447–457. doi:10.1016/S0006-2952(02)01521-6
13. Allenmark S (2003) Induced circular dichroism by chiral molecular interaction. Chirality 15:409–422. doi:10.1002/chir.10220
14. Haywar LD, Totty RN (1969) Induced optical rotation and circular dichroism of symmetric and racemic aliphatic carbonyl compounds. J Chem Soc D Chem Commun 676–677. doi:10.1039/C29690000676
15. Cainelli G, Galletti P, Pieraccini S, Quintavalla A, Giacomini D, Spada G (2004) Chiral aldehydes in hydrocarbons: diastereoselective nucleophilic addition, NMR, and CD spectroscopy reveal dynamic solvation effects. Chirality 16:50–56. doi:10.1002/chir.10310
16. Zsila F, Iwao Y (2007) The drug binding site of human alpha1-acid glycoprotein: insight from induced circular dichroism and electronic absorption spectra. Biochim Biophys Acta 1770:797–809. doi:10.1016/j.bbagen.2007.01.009
17. Pistolozzi M, Bertucci C (2008) Species-dependent stereoselective drug binding to albumin: a circular dichroism study. Chirality 20:552–558. doi:10.1002/chir.20521
18. Khouri SJ, Knierim R, Buss V (2009) Induced circular dichroism of the interaction between pinacyanol and algal alginates. Carbohydrate Res 344:1729–1733. doi:10.1016/j.carres.2009.06.026
19. Zhao P, Xu LC, Huang JW, Zheng KC, Fu B, Yu HC, Ji LN (2008) Tricationic pyridium porphyrins appending different peripheral substituents: experimental and DFT studies on their interactions with DNA. Biophys Chem 135:102–109. doi:10.1016/j.bpc.2008.03.013
20. Carmona T, Gonzalez-Alvarez MJ, Mendicuti F, Tagliapietra S, Martina K, Cravotto G (2010) Structure and self-aggregation of mono- and bis(cyclodextrin) derivatives in aqueous media: fluorescence, induced circular dichroism and molecular dynamics. J Phys Chem C 114:22431–22440. doi:10.1021/jp107221z
21. Zhang X, Nau WM (2000) Chromophore Alignment in a Chiral Host Provides a Sensitive Test for the Orientation-Intensity Rule of Induced Circular Dichroism. Angew Chem Int Ed 39:544–547. doi:10.1002/(SICI)1521-3773(20000204)39:3<544::AID-ANIE544>3.0.CO;2-#
22. Matei I, Soare L, Tablet C, Hillebrand M (2009) Characterization of simvastatin and its cyclodextrin inclusion complexes by absorption and circular dichroism spectroscopies and molecular mechanics calculations. Rev Roum Chim 54:133–141
23. Nakagawa H, Kobori Y, Yamada KI (2001) Spontaneous chirality conversion of [5]thiaheterohelicene in charge-transfer complexes in SDS micelles. Chirality 13:722–726. doi:10.1002/chir.10009
24. Matei I, Hillebrand M (2010) Interaction of kaempferol with human serum albumin: a fluorescence and circular dichroism study. J Pharm Biomed Anal 51:768–773. doi:10.1016/j.jpba.2009.09.037
25. Matei I, Ionescu S, Hillebrand M (2011) Interaction of fisetin with human serum albumin by fluorescence, circular dichroism spectroscopy and DFT calculations: binding parameters and conformational changes. J Lumin 131:1629–1635. doi:10.1016/j.jlumin.2011.03.073
26. Becke AD (1993) Density-functional thermochemistry. III. The role of exact exchange. J Chem Phys 98:5648–5642. doi:10.1063/1.464913
27. Stephens PJ, Devlin FJ, Chablowski CF, Frisch MJ (1994) Ab initio calculation of vibrational absorption and circular dichroism spectra using density functional force fields. J Phys Chem 98:11623–11627. doi:10.1021/j100096a001
28. Hertwig RH, Koch W (1997) On the parameterization of the local correlation functional. What is Becke-3-LYP? Chem Phys Lett 268:345–351. doi:10.1016/S0009-2614(97)00207-8
29. Frisch MJ, Trucks GW, Schlegel HB, Scuseria GE, Rob MA, Cheeseman JR, Montgomery JA Jr, Vreven T, Kudin KN, Burant JC, Millam JM, Iyengar SS, Tomasi J, Barone V, Mennucci B, Cossi M, Scalmani G, Rega N, Petersson GA, Nakatsuji H, Hada M, Ehara M, Toyota K, Fukuda R, Hasegawa J, Ishida M, Nakajima T, Honda Y, Kitao O, Nakai H, Klene M, Li X, Knox JE, Hratchian HP, Cross

JB, Bakken V, Adamo C, Jaramillo J, Gomperts R, Stratmann RE, Yazyev O, Austin AJ, Cammi R, Pomelli C, Ochterski JW, Ayala PY, Morokuma K, Voth GA, Salvador P, Dannenberg JJ, Zakrzewski VG, Dapprich S, Daniels AD, Strain MC, Farkas O, Malick DK, Rabuck AD, Raghavachari K, Foresman JB, Ortiz JV, Cui Q, Baboul AG, Clifford S, Cioslowski J, Stefanov BB, Liu G, Liashenko A, Piskorz P, Komaromi I, Martin RL, Fox DJ, Keith T, Al-Laham MA, Peng CY, Nanayakkara A, Challacombe M, Gill PMW, Johnson B, Chen W, Wong MW, Gonzalez C, Pople JA (2003) Gaussian 03. Gaussian Inc, Wallingford

30. Tomasi J, Mennucci B, Cammi R (2005) Quantum mechanical continuum solvation models. Chem Rev 105:2999–3093. doi:10.1021/cr9904009
31. Allouche AR (2011) Gabedit - A graphical user interface for computational chemistry softwares. J Comput Chem 32:174–182. doi:10.1002/jcc.21600
32. Herrero-Martinez JM, Sanmartin M, Roses M, Bosch E, Rafols C (2005) Determination of dissociation constants of flavonoids by capillary electrophoresis. Electrophoresis 26:1886–1895. doi:10.1002/elps.200410258
33. Bhat SV, Nagasampagi BA, Sivakumar M (2006) Chemistry of natural products. Springer, Berlin
34. Sortino S, Petralia S, Condorelli G, Marconi G (2003) Direct spectroscopic evidence that the photochemical outcome of flutamide in a protein environment is tuned by modification of the molecular geometry: a comparison with the photobehavior in cyclodextrin and vesicles. Helvetica Chim Acta 86:266–273. doi:10.1002/hlca.200390027
35. Whitmore L, Wallace BA (2008) Protein secondary structure analyses from circular dichroism spectroscopy: methods and reference databases. Biopolymers 89:392–400. doi:10.1002/bip.20853
36. Zsila F, Bikadi Z, Fitos I, Simonyi M (2004) Probing protein binding sites by circular dichroism spectroscopy. Curr Drug Discov Technol 1:133–153
37. Cramer CJ (2004) Essentials of computational chemistry theories and models, 2nd edn. Wiley, Chichester, pp 280–290
38. Tawada Y, Tsuneda T, Yanagisawa S, Yanai T, Hirao K (2004) A long-range-corrected time-dependent density functional theory. J Chem Phys 120:8425–8433. doi:10.1063/1.1688752
39. Chaudhuri S, Chakraborty S, Sengupta PK (2011) Probing the interactions of hemoglobin with antioxidant flavonoids via fluorescence spectroscopy and molecular modeling studies. Biophys Chem 154:26–34. doi:10.1016/j.bpc.2010.12.003